






Can Cuspy Dark-matter-dominated Halos Hold Cored Stellar Mass Distributions?

Jorge Sánchez Almeida^{1,2} , Angel R. Plastino³ , and Ignacio Trujillo^{1,2} ¹Instituto de Astrofísica de Canarias, La Laguna, Tenerife, E-38200, Spain; jos@iac.es²Departamento de Astrofísica, Universidad de La Laguna, Spain³CeBio y Departamento de Ciencias Básicas, Universidad Nacional del Noroeste de la Provincia de Buenos Aires, UNNOBA, CONICET, Roque Saenz Peña 456, Junin, Argentina

Received 2023 April 17; revised 2023 June 26; accepted 2023 July 2; published 2023 September 8

Abstract

According to the current concordance cosmological model, dark matter (DM) particles are collisionless and produce self-gravitating structures with a central cusp, which, generally, is not observed. The observed density tends to a central plateau or core, explained within the cosmological model through the gravitational feedback of baryons on DM. This mechanism becomes inefficient when decreasing the galaxy's stellar mass so that in the low-mass regime ($M_* \ll 10^6 M_\odot$) the energy provided by the baryons is insufficient to modify cusps into cores. Thus, if cores exist in these galaxies they have to reflect departures from the collisionless nature of DM. Measuring the DM mass distribution in these faint galaxies is extremely challenging; however, their stellar mass distribution can be characterized through deep photometry. Here we provide a way of using only the stellar mass distribution to constrain the underlying DM distribution. The so-called Eddington inversion method allows us to discard pairs of stellar distributions and DM potentials requiring (unphysical) negative distribution functions in the phase space. In particular, cored stellar density profiles are incompatible with the Navarro–Frenk–White (NFW) potential expected from collisionless DM if the velocity distribution is isotropic and the system spherically symmetric. Through a case-by-case analysis, we are able to relax these assumptions to consider anisotropic velocity distributions and systems that do not have exact cores. In general, stellar distributions with radially biased orbits are difficult to reconcile with NFW-like potentials, and cores in the baryon distribution tend to require cores in the DM distribution.

Unified Astronomy Thesaurus concepts: Cold dark matter (265); Dwarf galaxies (416); Galaxy mass distribution (606); Navarro–Frenk–White profile (1091); Galaxy dark matter halos (1880); Low surface brightness galaxies (940); Theoretical techniques (2093)

1. Introduction

The current concordance cosmological model assumes that dark matter (DM) particles are cold and collisionless (e.g., White & Rees 1978; Blumenthal et al. 1984; Davis et al. 1985; Smoot et al. 1992; Peebles 2021; Bechtol et al. 2022). Thus, cold dark matter (CDM) particles interact with themselves and with the baryons through gravitational forces only. Given the initial conditions set by the cosmological model, CDM particles evolve under their own gravity to collapse into halos with cusps (e.g., Cen 2014; Brown et al. 2020), i.e., where the density is represented by the iconic Navarro–Frenk–White (NFW) profile (Navarro et al. 1997), which grows boundlessly when approaching the center of the gravitational potential. This prediction is in contrast with the fact that the observed DM halos often show cores, i.e., their density tends to be constant as one approaches the center (e.g., Weinberg et al. 2015; Bullock & Boylan-Kolchin 2017; Del Popolo & Le Delliou 2017). This apparent contradiction is solved within the current CDM paradigm because the baryon dynamics modifies the global gravitational potential also affecting the DM distribution and transforming the cusps into cores (Davis et al. 1992; Governato et al. 2010; Di Cintio et al. 2014b). This mechanism of feedback of baryons onto DM becomes inefficient when decreasing the galaxy mass because the halo-to-stellar mass

ratio increases with decreasing mass (e.g., Behroozi et al. 2013), reaching a point where the energy provided by star formation is simply not enough to modify the cusp of CDM halos (e.g., Peñarrubia et al. 2012; Oñorbe et al. 2015). The larger stellar mass unable to modify the inner slope of the DM profile is somewhat model dependent (e.g., Read et al. 2016), but it roughly corresponds to stellar masses $M_* < 10^6 M_\odot$ or halo masses $M_h < 10^{10} M_\odot$ (e.g., Di Cintio et al. 2014b; Chan et al. 2015; Hayashi et al. 2020; Jackson et al. 2021; Expósito-Márquez et al. 2023). Thus, if galaxies with $M_h \ll 10^{10} M_\odot$ show DM cores, they are not due to baryon feedback but have to reflect the nature of DM: whether it is fuzzy, self-interacting, warm, or else (e.g., Dodelson & Widrow 1994; Hu et al. 2000; Spergel & Steinhardt 2000; Bechtol et al. 2022).

At these low masses, discerning observationally whether DM halos have cores is extremely challenging, if not impossible. DM measurements require high spectral resolution spectroscopy to infer dynamical masses (whether optical, infrared, or radio wavelengths are used). The light is spread into small wavelength bins and so getting high signal-to-noise ratios is expensive observationally. On the contrary, stellar mass determinations depend on broadband photometry, which is orders of magnitude faster than spectroscopy. Thus, measuring the baryon mass distribution in these low-mass objects is doable (e.g., Trujillo et al. 2021), and interestingly, low-mass galaxies tend to show cores in their stellar mass distribution (e.g., Moskowit & Walker 2020; Carlsten et al. 2021). Since low-mass galaxies are often extremely DM-dominated systems, one could naively think that the cores



Original content from this work may be used under the terms of the [Creative Commons Attribution 4.0 licence](https://creativecommons.org/licenses/by/4.0/). Any further distribution of this work must maintain attribution to the author(s) and the title of the work, journal citation and DOI.

Table 1
Summary of the Compatibility Between the Baryon Density Profile and the Potential

Baryons and Potential, Velocity (1)	Consistency (2)	Comments (3)	Section (4)
Core ^a and NFW ^b , isotropic	X	Equations (23) and (24). $\beta = 0^c$. Figure 1	Section 3
Power law ^d and power law, isotropic	?	$\alpha > 0^d$ ✓ $\alpha < 0$ X. Equation (25). $\beta = 0$	Sections 3, 4.2
Core and soft core ^e , isotropic	X	$\beta = 0$. Figure 3. Figure 4	Section 4.2, Appendix E
Core and core, isotropic	?	$\beta = 0$. $a \leq 2$ ✓ $a > 2$ X. Figure 6	Sections 4.1, 4.2, Appendix E
Soft core and NFW, isotropic	?	$\beta = 0$. Figures 4, 5. $c \gtrsim 0.1$ ✓ $c \lesssim 0.1$ X.	Sections 3, 4.2
Soft core and soft core, isotropic	?	$\beta = 0$. Figures 4, 5	Sections 3, 4.2
Core and NFW, O-M model	X	$r_s \gtrsim 2 r_{sp}$ X, $c > c_p$ ✓ $\beta (\neq 0)$ in Equation (12)	Section 4.2
Core and NFW, radially biased	X	Constant β . $\beta > 0$	Section 3, Appendix D
Core and Any, radially biased	X	Constant β . $\beta > 0$	Section 3, Appendix D
Power law and any, anisotropic	?	Constant β . $\alpha > 2\beta$	Section 3, Appendix D
Core and NFW, circular	✓	$\beta = -\infty$	Appendix C
Any and any, circular	✓	$\beta = -\infty$	Appendix C
Any and any, tangentially biased	?	$\beta < 0$. Equation (18). $f_i < 0$ X	Sections 2.3, 3

Notes. (1) Description of the baryon density, the gravitational potential, and the velocity distribution. (2) The symbols ✓, X, and ? stand for compatible, incompatible, and may or may not, respectively. (3) Additional comments and keywords. (4) Section of the text where the combination described in (1) is discussed.

^a Core $\equiv d \log \rho / d \log r \rightarrow 0$ when $r \rightarrow 0$.

^b NFW potential (Equation (A6)) produced by an NFW profile (Equation (A5)).

^c Velocity anisotropy parameter β defined in Equation (11).

^d $\rho \propto r^{-\alpha}$.

^e Soft cores defined in Equations (30) and (32), and illustrated in Figure 2. Power laws ^d are a particular type of those.

observed in stars just reflect the underlying DM mass distribution. If this conjecture turned out to be correct, it would provide a unique channel to study DM in low-mass galaxies, in a regime particularly informative to reveal the nature of DM (e.g., Weinberg et al. 2015; Bullock & Boylan-Kolchin 2017; Del Popolo & Le Delliou 2017). Thus, the question arises as to whether or not the cores in the stellar mass distribution of DM-dominated systems trace cores in the DM distribution.

The purpose of this work is to raise the question in the title and answer it in fairly broad terms. Thus, we show that is unlikely (although not impossible) that DM-dominated systems with a central cusp have a stellar profile with a central core. Therefore, our work provides a gateway to investigate the inner shape of the DM distribution in ultralow-mass galaxies using only their starlight.

We address the question using the so-called Eddington inversion method (Eddington 1916; Binney & Tremaine 2008; Lacroix et al. 2018). Simply put, it provides the distribution function (DF) in the phase-space f corresponding to a stellar mass density distribution ρ immersed in a gravitational potential Φ . Given two arbitrary ρ and Φ , there is no guarantee that $f > 0$ everywhere, which is the absolute minimum requirement for ρ and Φ to be physically consistent. In this paper, we study the f resulting from different combinations of ρ (tracing the stars) and Φ (dictated only by the DM in ultralow-mass galaxies). We will show that unless the potential Φ is created by a mass distribution with a core, cored ρ s often give nonphysical $f < 0$. The computations in the paper neglect the contribution of the baryons to the overall potential, which we regard as a reasonable working hypothesis for the galaxies of interest. Thus, the gas in ultralow-mass galaxies is not treated explicitly in this paper, but should play only a minor role in the analysis since it interacts with the stars only through its contribution to the gravitational potential. Therefore, as soon as

the gas mass is much smaller than the total mass of the system, its presence can be neglected.

The paper is organized as follows: Section 2 puts forward the Eddington inversion method together with the main equations used in our analysis. The more lengthy derivations are presented separately in Appendices A–E. Unphysical pairs $\rho - \Phi$ yielding $f < 0$ somewhere are analyzed in Section 3, among which one finds the prototypical cored ρ immersed in an NFW potential with isotropic velocities. Examples and particular cases are worked out in Section 4 to conclude that most often the cores in baryons trace DM cores in DM-dominated self-gravitating systems. These results and their practical application to real galaxies are analyzed in Section 5, including the effect of relaxing assumptions like spherical symmetry. Table 1 lists consistent and inconsistent combinations of ρ and Φ resulting from our analysis. In what follows, we use the terms baryons, stars, or particles indistinctly to refer to the component of the gravitationally bound system that provides the density ρ . Moreover, in the context of this paper, the term low-mass galaxy is used to describe galaxies where the potential is approximately set by the DM because the gravity produced by the baryons can be neglected.

2. The Eddington Inversion Method in Our Context

This section provides a summary of the Eddington inversion method, and so, of the expressions used in Sections 3 and 4 to study whether cored baryon density distributions happen to be inconsistent with the gravitational potential created by CDM alone. We closely follow the approach and terminology by Binney & Tremaine (2008, Section 4.3), but there are several alternative references on the subject (e.g., Ciotti & Pellegrini 1992; Ciotti 1996; Lacroix et al. 2018). The main assumptions made when using the Eddington inversion method are (Binney & Tremaine 2008, Section 4): (1) the gravitational potential is smooth, (2) the trace particles (e.g., stars) have lifetimes larger than the crossing time, (3) the trace particles are

collisionless, (4) the system is spherically symmetric, and (5) the system is described by a steady-state DF in the phase space. We take these assumptions as working hypotheses, which may not be fulfilled by particular objects but may be good enough to describe large populations. For example, after a major merger, the steady state may require a few Gyrs to recover (e.g., Lotz et al. 2008); however, most galaxies only have a few such events during their lifetimes concentrated early on, therefore, many galaxies should be in a quasi-steady state today. Based on these premises, we first consider particle systems with an isotropic velocity distribution. Section 2.1 explains how to use the Eddington inversion method to recover the phase-space DF from the three first spatial derivatives of the baryon density and of the gravitational potential. The general expressions are particularized to specific mass distributions and gravitational potentials in Appendices A.1 and A.2. Section 2.2 relaxes the assumption on the velocity isotropy, working out the expression of the DF for the Osipkov–Merritt velocity anisotropy model. Other anisotropic velocity models are considered too. Even if contrived from a physical standpoint, any gravitational potential is consistent with any density if the particles are arranged in perfectly circular orbits. The mixing model in Section 2.3 describes the linear superposition of such a DF with circular orbits plus another DF with an isotropic velocity distribution. Finally, Section 2.4 treats the case of constant velocity anisotropy.

These physical systems and the corresponding DFs were chosen for simplicity because they provide clear-cut constraints on the potential with relatively simple arguments. There are extensions of the Eddington inversion method for other more general DFs that in principle could be used for similar diagnostics (e.g., Lynden-Bell 1962; Dejonghe 1987; Cuddeford 1991; Strigari et al. 2017), but their study remains to be carried out, a task that requires specific follow-up work (Section 5).

2.1. Systems with Isotropic Velocity Distribution

For spherically symmetric systems of particles with isotropic velocity distribution, the phase-space DF $f(\epsilon)$ depends only on the particle energy ϵ . Then, the space density $\rho(r)$ turns out to be (Binney & Tremaine 2008, Section 4.3),

$$\rho(r) = 4\pi\sqrt{2} \int_0^{\Psi(r)} f(\epsilon) \sqrt{\Psi(r) - \epsilon} d\epsilon. \quad (1)$$

Here $\epsilon = \Psi - \frac{1}{2}v^2$ is the relative energy (per unit mass) of a particle, and $\Psi(r) = \Phi_0 - \Phi(r)$ is the relative potential energy, where $\Phi(r)$ is the gravitational potential energy and Φ_0 is the gravitational potential energy evaluated at the edge of the system. For realistic systems, the relative potential Ψ is a monotonically decreasing function of the distance from the center r . Consequently, ρ can be regarded as a function of Ψ . Differentiating ρ with respect to Ψ ,

$$\frac{d\rho}{d\Psi} = 2\pi\sqrt{2} \int_0^{\Psi} \frac{f(\epsilon)}{\sqrt{\Psi - \epsilon}} d\epsilon. \quad (2)$$

Inverting this Abel integral leads to Eddington’s celebrated equation (e.g., Binney & Tremaine 2008, Equation (4.46)) for the phase-space DF $f(\epsilon)$ in terms of the spatial density $\rho(r)$,

$$f(\epsilon) = \frac{1}{2\sqrt{2}\pi^2} \frac{d}{d\epsilon} \int_0^{\epsilon} \frac{d\rho}{d\Psi} \frac{d\Psi}{\sqrt{\epsilon - \Psi}}. \quad (3)$$

Integrating by parts twice,

$$f(\epsilon) = \frac{1}{\sqrt{2}\pi^2} \left[\frac{1}{2\sqrt{\epsilon}} \left(\frac{d\rho}{d\Psi} \right)_{\Psi=0} + \sqrt{\epsilon} \left(\frac{d^2\rho}{d\Psi^2} \right)_{\Psi=0} + \int_0^{\epsilon} \frac{d^3\rho}{d\Psi^3} \sqrt{\epsilon - \Psi} d\Psi \right]. \quad (4)$$

The derivatives at the boundary, $(d\rho/d\Psi)_{\Psi=0}$ and $(d^2\rho/d\Psi^2)_{\Psi=0}$, are in practice zero (see Appendix B); therefore,

$$f(\epsilon) = \frac{1}{\sqrt{2}\pi^2} \int_0^{\epsilon} \frac{d^3\rho}{d\Psi^3} \sqrt{\epsilon - \Psi} d\Psi. \quad (5)$$

To evaluate numerically the integral appearing in Equation (5), it is convenient to change the integration variable from Ψ to r , because only $\rho(r)$ and $\Psi(r)$ are known explicitly. To use r as an integration variable, we need to express the derivatives of ρ with respect to Ψ in terms of the derivatives of ρ and Ψ with respect to r , i.e.,

$$\frac{d\rho}{d\Psi} = \frac{d\rho/dr}{d\Psi/dr}, \quad (6)$$

$$\frac{d^2\rho}{d\Psi^2} = \left(\frac{d\Psi}{dr} \right)^{-3} \left[\left(\frac{d^2\rho}{dr^2} \right) \left(\frac{d\Psi}{dr} \right) - \left(\frac{d\rho}{dr} \right) \left(\frac{d^2\Psi}{dr^2} \right) \right], \quad (7)$$

$$\begin{aligned} \frac{d^3\rho}{d\Psi^3} &= \left(\frac{d^3\rho}{dr^3} \right) \left(\frac{d\Psi}{dr} \right)^{-3} - 3 \left(\frac{d^2\rho}{dr^2} \right) \left(\frac{d^2\Psi}{dr^2} \right) \left(\frac{d\Psi}{dr} \right)^{-4} \\ &\quad - \left(\frac{d\rho}{dr} \right) \left(\frac{d^3\Psi}{dr^3} \right) \left(\frac{d\Psi}{dr} \right)^{-4} \\ &\quad + 3 \left(\frac{d\rho}{dr} \right) \left(\frac{d^2\Psi}{dr^2} \right)^2 \left(\frac{d\Psi}{dr} \right)^{-5}. \end{aligned} \quad (8)$$

We now change the integration variable in the integral appearing in Equation (5),

$$\begin{aligned} \int_0^{\epsilon} \frac{d^3\rho}{d\Psi^3} \sqrt{\epsilon - \Psi} d\Psi &= \int_{r_m}^R \frac{d\Psi}{dr} \frac{d^3\rho}{d\Psi^3} \sqrt{\epsilon - \Psi} dr \\ &= - \int_R^{r_m} \frac{d\Psi}{dr} \frac{d^3\rho}{d\Psi^3} \sqrt{\epsilon - \Psi} dr, \end{aligned} \quad (9)$$

where R is the value of r such that $\Psi(R) = \epsilon$, and r_m is the maximum value of r , corresponding to the outer edge of the system. When the system has infinite spatial extent $r_m \rightarrow \infty$. Replacing expression (8) for $d^3\rho/d\Psi^3$ into the integral in Equation (9),

$$\begin{aligned} \int_0^{\epsilon} \frac{d^3\rho}{d\Psi^3} \sqrt{\epsilon - \Psi} d\Psi &= \int_R^{r_m} \left[- \left(\frac{d^3\rho}{dr^3} \right) \left(\frac{d\Psi}{dr} \right)^{-2} \right. \\ &\quad + 3 \left(\frac{d^2\rho}{dr^2} \right) \left(\frac{d^2\Psi}{dr^2} \right) \left(\frac{d\Psi}{dr} \right)^{-3} \\ &\quad + \left(\frac{d\rho}{dr} \right) \left(\frac{d^3\Psi}{dr^3} \right) \left(\frac{d\Psi}{dr} \right)^{-3} \\ &\quad \left. - 3 \left(\frac{d\rho}{dr} \right) \left(\frac{d^2\Psi}{dr^2} \right)^2 \left(\frac{d\Psi}{dr} \right)^{-4} \right] \\ &\quad \sqrt{\epsilon - \Psi} dr. \end{aligned} \quad (10)$$

In short, according to Equations (5) and (10), the DF $f(\epsilon)$ corresponding to a density $\rho(r)$ in a potential $\Phi(r)$ can be

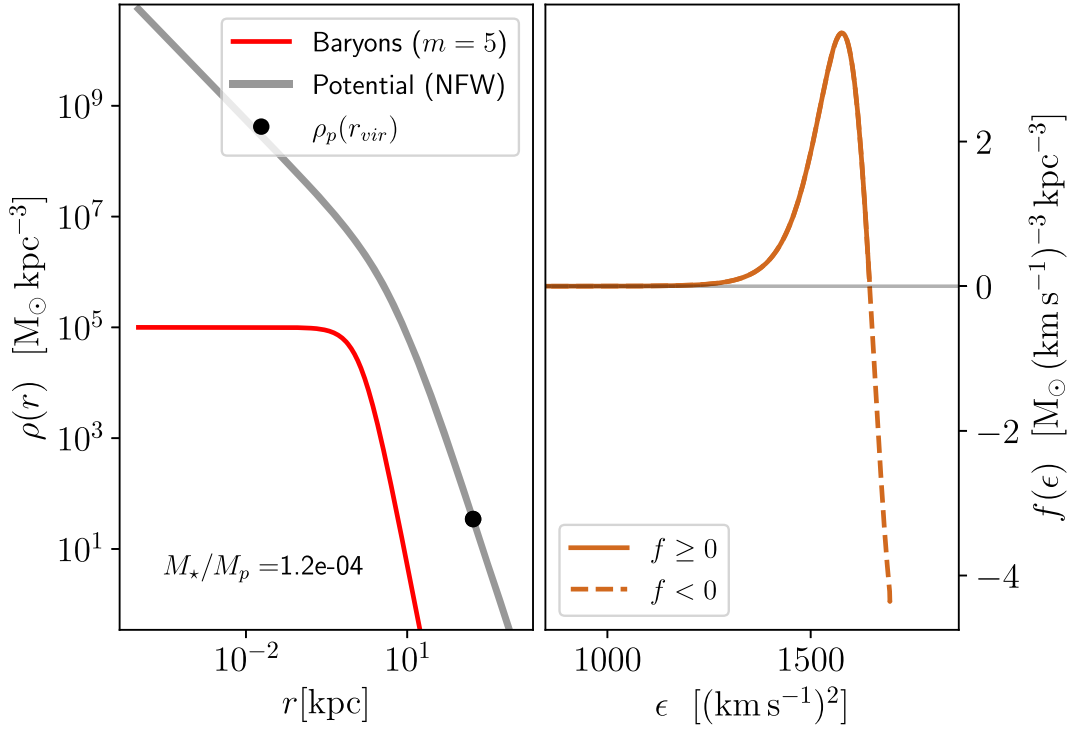


Figure 1. Cored baryon distribution in an NFW gravitational potential. Left panel: a polytrope of order $m = 5$ gives $\rho(r)$, with the central density $\rho(0) = 10^5 M_\odot \text{ kpc}^{-3}$ and a core radius $r_0 = 1.4 \text{ kpc}$, chosen so that $M_* \sim 10^6 M_\odot$ (the red solid line). The NFW density profile that defines the overall gravitational potential through the Poisson equation (the gray line) has $\rho_s/\rho(0) = 10$ and $r_s/r_0 = 4$, which provides $M_*/M_p \simeq 1.2 \times 10^{-4}$. The bullet symbol points out the total density at the virial radius, assuming a concentration of 30 ($r_{\text{vir}} = 30 r_s$). Right panel: baryon DF f needed to match baryon density and potential according to Eddington’s inversion method which reaches negative values (the dashed line) implying that this particular combination is unphysical.

deduced from the first three derivatives of $\rho(r)$ and $\Psi(r)$ ($=\Phi_0 - \Phi$). Appendix A works them out in various practical cases involving polytropic ρ and NFW densities and potentials. Examples of ρ and $f(\epsilon)$ will be shown in Section 4, Figures 1–3, 5, and 6.

2.2. Systems with Anisotropic Velocity Distribution: the Osipkov–Merritt Model

The systems described in Section 2.1 have DFs depending on the particle energy only, which holds when the dispersion of velocities in the three independent spatial directions is the same. In terms of the so-called anisotropy parameter, these systems have $\beta(r) = 0$, with

$$\beta(r) = 1 - \frac{\sigma_\theta^2 + \sigma_\phi^2}{2\sigma_r^2}, \quad (11)$$

where σ_r is the radial velocity dispersion, and σ_θ and σ_ϕ are the tangential velocity dispersions in spherical coordinates. The velocity isotropy requirement can be relaxed assuming f to depend not only on ϵ but also on the modulus of the angular momentum L . This is done in the Osipkov–Merritt model, which assumes a radial dependence of the anisotropy given by

$$\beta(r) = \frac{r^2}{r^2 + r_b^2}, \quad (12)$$

where the anisotropy radius r_b sets the spatial scale of the changes in anisotropy. For $r \ll r_b$ the velocity distribution is isotropic, while for $r \gg r_b$ it is fully anisotropic with $\beta \rightarrow 1$ and the orbits becoming mostly radial ($\sigma_\theta^2 + \sigma_\phi^2 \ll 2\sigma_r^2$). The assumption on $\beta(r)$ in the Osipkov–Merritt model (Equation (12)) may look

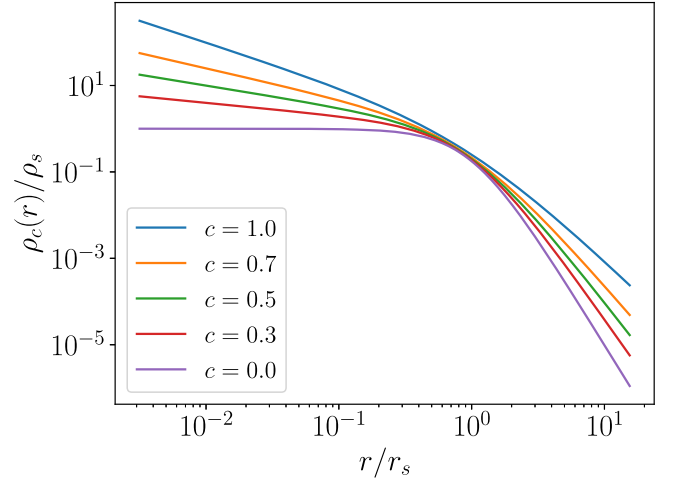


Figure 2. Double power-law density profile (Equation (32)) that goes seamlessly from a Schuster–Plummer profile to an NFW profile when the inner slope ($-c$) goes from 0 to -1 .

artificial, driven by analytical simplicity, but this is not quite so. This type of radial dependence of the anisotropy parameter is obtained in cosmological numerical simulations of galaxy formation in the low-mass end of the mass spectrum (e.g., El-Badry et al. 2017; Orkney et al. 2023). In these simulations, the stars tend to have isotropic orbits in the center of the potential that turn into radial orbits in the outskirts. In the same numerical simulations, the DM halos are more isotropic all over (discussed further in Section 5).

Following Binney & Tremaine (2008), the phase-space DF of the Osipkov–Merritt model depends on the particle position

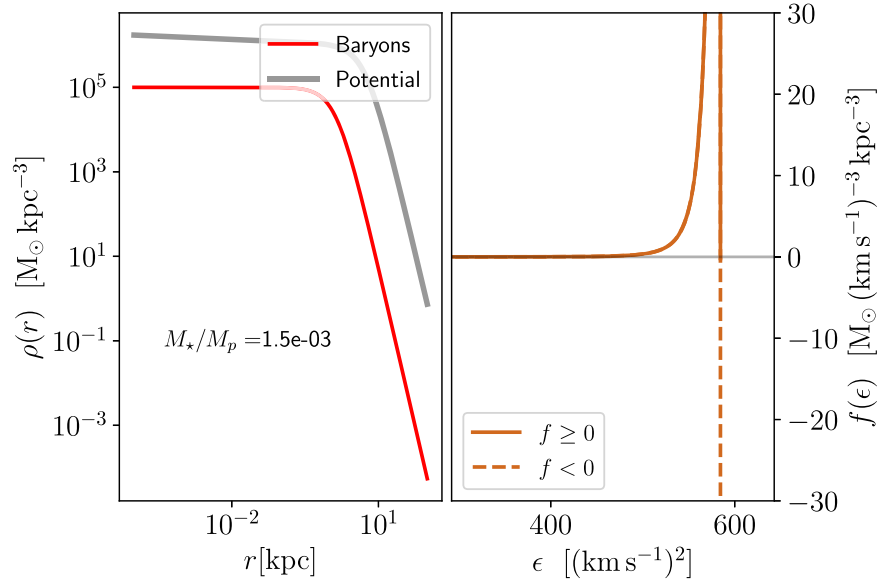


Figure 3. Similar to Figure 1 but this time only with a hint of cusp in the density that generates the potential: $c = 0$ and $c_p = 0.05$. Note that $f < 0$ at large ϵ , implying that density and potential are inconsistent with each other.

and velocity through the quantity

$$Q = \epsilon - \frac{L^2}{2r_b^2}. \quad (13)$$

It is convenient to define

$$\rho_{\text{OM}}(r) = \left(1 + \frac{r^2}{r_b^2}\right) \rho(r). \quad (14)$$

The connection between the mass density and the phase-space density can be expressed, in terms of ρ_{OM} , in a way similar to the one corresponding to isotropic systems. Indeed, one has

$$\rho_{\text{OM}}(r) = 4\pi\sqrt{2} \int_0^{\Psi(r)} f_{\text{OM}}(Q) \sqrt{\Psi(r) - Q} dQ, \quad (15)$$

$$\frac{d\rho_{\text{OM}}}{d\Psi} = 2\sqrt{2}\pi \int_0^{\Psi} \frac{f_{\text{OM}}(Q)}{\sqrt{\Psi - Q}} dQ, \quad (16)$$

and

$$f_{\text{OM}}(Q) = \frac{1}{2\sqrt{2}\pi^2} \frac{d}{dQ} \int_0^Q \frac{d\rho_{\text{OM}}}{d\Psi} \frac{d\Psi}{\sqrt{Q - \Psi}}. \quad (17)$$

Therefore, expressions (5)–(10) also hold in this case replacing ρ with ρ_{OM} and ϵ with Q .

2.3. Systems with Anisotropic Velocity Distribution: The Mixing Model

A particle system having only circular orbits has always a radial velocity equal to zero, and so, $\sigma_r = 0$, which leads to $\beta = -\infty$ everywhere. A system with such an extreme velocity anisotropy can reproduce any pair potential–density with a DF, denoted here as f_c , guaranteed to be positive everywhere (see Appendix C). A fairly general system with anisotropic velocity distribution can be constructed as a linear superposition of a system with circular orbits f_c and a system with isotropic velocity distribution f_i (Binney & Tremaine 2008), so

that

$$f(\mathbf{r}, \mathbf{v}) = \mu f_i[\Psi(r) - v^2/2] + (1 - \mu) f_c[\mathbf{r}, v_r, v_\theta, v_\phi], \quad (18)$$

with \mathbf{r} and \mathbf{v} the position and velocity in the 6D phase space and μ parameterizing the mixing fraction ($0 \leq \mu \leq 1$). The symbols v_r , v_θ , and v_ϕ represent the three coordinates of the velocity vector in a reference system where v_r is the component in the radial direction set by \mathbf{r} . Equation (18) explicitly shows that f_i depends on the velocity through $v^2 = v_r^2 + v_\theta^2 + v_\phi^2$, a property used in Section 3 to discuss the feasibility of DFs from the mixing model. In this case, the anisotropy parameter at a fixed radius is

$$\beta = -\frac{1 - \mu}{\mu} \frac{\sigma_\theta^2 + \sigma_\phi^2|_c}{\sigma_\theta^2 + \sigma_\phi^2|i} \leq 0, \quad (19)$$

where σ_θ and σ_ϕ stand for the velocity dispersion in the two tangential coordinates and $|_i$ and $|_c$ point out the isotropic and the circular velocity DF, respectively. The resulting orbits are between circularly biased and isotropic, but never radially biased.

2.4. Systems with Anisotropic Velocity Distribution: Constant Velocity Anisotropy

An extension of the above Eddington formalism deals with anisotropic velocity distributions of constant β . One starts from the DF,

$$f(\epsilon, L) = L^{-2\beta} f_\epsilon(\epsilon), \quad (20)$$

which represents a leading order approximation for a wide class of DFs having the anisotropy parameter β constant (An & Evans 2006; Binney & Tremaine 2008). In these systems, the DF depends not only on the relative energy ϵ but also on the modulus of the angular momentum L . Under this assumption, the mass volume density can be written as (Binney &

Tremaine 2008, Equation (4.66)),

$$r^{2\beta}\rho(r) = \kappa_\beta \int_0^\Psi \frac{f_\epsilon(\epsilon)}{(\Psi - \epsilon)^{\beta-1/2}} d\epsilon, \quad (21)$$

where κ_β is a positive numerical value independent of the radius r . Note that this equation is formally quite similar to Equation (1) provided $\beta < 1/2$, and so will be used in Section 3 to point out the inconsistency of a large number of densities and potentials in a way that parallels the isotropic case. This DF is also closely connected to the so-called cusp slope-central anisotropy theorem by An & Evans (2006), which links the inner slope of a density profile with the velocity anisotropy. This is examined in our context in Appendix D.

3. Positivity of the Phase-space DF

Positivity is the basic requirement for any physically sensible phase-space distribution. Given a relative potential function Ψ and a mass density profile ρ , it is not guaranteed that the phase-space distribution yielded by the Eddington inversion method is positive everywhere in the phase space. A negative DF implies that the assumptions made when applying Eddington's method are physically inconsistent: there is no phase-space DF that can reproduce the mass density ρ under the assumed potential Ψ . We use this idea here and in Section 4 to analyze the consistency of several combinations of Ψ and ρ that may be of practical importance.

Requiring f to be non-negative constrains the properties of the centers of low-mass galaxies in fairly general terms. Equation (2) leads to a sufficient condition for the physical incompatibility between $\rho(r)$ and $\Psi(r)$ (e.g., Lacroix et al. 2018). If, for a given Ψ (and consequently, a given r), $d\rho/d\Psi$ vanishes, then, it follows from Equation (2) that the phase-space density $f(\epsilon)$ yielded by the Eddington method must reach negative values. (For the integral in Equation (2) to be zero with $f(\epsilon) \neq 0$, $f(\epsilon) < 0$ somewhere within the interval $0 \leq \epsilon \leq \Psi$.) Thus, if $d\rho/d\Psi = 0$ somewhere, then no isotropic distribution is compatible with the given $\rho(r)$ and $\Psi(r)$. Taking into account the relation

$$\frac{d\rho}{d\Psi} = \frac{d\rho/dr}{d\Psi/dr}, \quad (22)$$

it follows that a cored mass density, defined as having

$$\lim_{r \rightarrow 0} \frac{d\rho}{dr} = 0, \quad (23)$$

is inconsistent with an NFW background potential, which has

$$\lim_{r \rightarrow 0} \frac{d\Psi}{dr} = -\frac{V_c}{2r_s^2} \neq 0; \quad (24)$$

see Equation (A8), with the constants V_c and r_s defined in Appendix A.1.

The condition for $f > 0$ derived above has a twist when the requirement of having a core (Equation (23)) is somewhat relaxed. Consider a power-law baryon density profile, $\rho \propto r^{-\alpha}$, with $\alpha = 0$ for a cored profile. Consider also a power law for the density profile generating the potential, $\rho_p \propto r^{-\alpha_p}$, with

$\alpha_p = 1$ for an NFW profile. The relative potential Ψ follows from ρ_p so that for $\alpha \neq 0$ one finds⁴

$$\frac{d\rho/dr}{d\Psi/dr} \simeq A \alpha r^{-(2+\alpha-\alpha_p)}, \quad (25)$$

with $A > 0$ provided $0 < \alpha_p < 3$. (The case $\alpha = 0$ is controlled by a second term to be added to the right-hand side (RHS) of Equation (25), and is treated in Appendix E.) Thus, the inconsistency between baryons and potential when $r \rightarrow 0$ disappears when $\alpha > 0$ since $(d\rho/dr)/(d\Psi/dr) \rightarrow \infty$ when $r \rightarrow 0$. Note, however, that f may still be negative somewhere else with $r \neq 0$ even when $\alpha > 0$, as we will show to be often the case (Section 4.2). Note also that all profiles with $\alpha < 0$ (i.e., density decreasing toward the center) are discarded for any potential since the derivative Equation (25) is either zero or negative when $r \rightarrow 0$.

The above results hold for systems where the velocity anisotropy is zero, however, they can be extended to other more general anisotropic systems. The Osipkov–Merritt model, which has an anisotropy parameter given by Equation (12), follows a relation for the DF (Equation (16)) formally identical to Equation (2). Provided the density profile has a core (i.e., provided it follows Equation (23)),

$$\lim_{r \rightarrow 0} \frac{d\rho_{\text{OM}}}{dr} = \lim_{r \rightarrow 0} \left(2r\rho/r_b^2 + [1 + r^2/r_b^2] \frac{d\rho}{dr} \right) = 0, \quad (26)$$

which implies that cored density profiles are incompatible with an NFW potential even when the velocity is anisotropic following an Osipkov–Merritt model. As we stress in Section 2.2, this model for the radial variation of the anisotropy parameter is not as contrived as one may think since it is roughly followed by the low-mass model galaxies resulting from cosmological numerical simulations of galaxy formation.

The constraints posed above happen to be a consequence of a more general cusp slope-central anisotropy theorem by An & Evans (2006). These authors showed that for systems with constant velocity anisotropy β (i.e., those described in Section 2.4), the need for the DF to be positive provides a constraint on the inner slope of the density profile α (i.e., $\rho \propto r^{-\alpha}$ when $r \rightarrow 0$),

$$\alpha \geq 2\beta. \quad (27)$$

This holds independently of the gravitational potential Ψ . As we show in Appendix D, when this is combined with the constraint in Equation (24) set by having an NFW background potential, it leads to

$$\alpha > 2\beta. \quad (28)$$

The inequality in Equation (28) has a number of implications: (1) cores ($\alpha = 0$) are inconsistent with isotropic velocities ($\beta = 0$), as we have shown already, (2) cores are inconsistent with radially biased orbits (i.e., only $\beta < 0$ is allowed for $\alpha = 0$), (3) radially biased orbits ($\beta > 0$) require cuspy baryon density profiles ($\alpha > 0$), and (3) circular orbits do not impose any restriction on the inner slope α since their $\beta = -\infty$. Actually, it is already known that strongly tangentially biased orbits can reconcile a cored stellar density profile with a cuspy

⁴ The relation is given explicitly in Section 4.2, Equations (33) and (35).

CDM-like background potential (Breddels & Helmi 2013, a Schuster–Plummer density profile in a Hernquist potential).

The constraint on galaxies having radially biased orbits ($\beta > 0$) is particularly important from a practical point of view since these orbits seem to be the natural outcome of the formation of dwarf galaxies in a Lambda CDM (Λ CDM) cosmological numerical simulations: see, e.g., (El-Badry et al. 2017, Figure 2) and (Orkney et al. 2023, Figure 5). Moreover, even if the uncertainties are large, values of $\beta \gtrsim 0$ are also observed among the DM-dominated satellites of the MW (e.g., Łokas 2009; Massari et al. 2018; Read et al. 2019; Massari et al. 2020; Leung et al. 2021; Kowalczyk & Łokas 2022).

There is also a fairly general family of tangentially biased DFs that can be discarded right away. It is described by the mixing model (Section 2.3) and covers the whole range of tangentially biased anisotropies from $\beta = -\infty$ to 0. The mixing model in Section 2.3 combines circular orbit DFs (f_c with $\beta = -\infty$) and isotropic velocity DFs (f_i with $\beta = 0$) to produce tangentially biased DFs with $\beta < 0$ (Equation (19)). One may naively think that the always positive f_c may compensate $f_i < 0$ to yield a positive physically sensible DF $f = \mu f_i + (1 - \mu) f_c$ (Equation (18)). However, all linear combinations can be discarded for any $\mu \neq 0$ if $f_i < 0$ somewhere. The argument goes as follows: assume that $f_i < 0$ at $\mathbf{r} = \mathbf{r}_1$ and $\mathbf{v} = \mathbf{v}_1 = (v_{r1}, v_{\theta1}, v_{\phi1})$ (see the dependencies of the DF on position \mathbf{r} and velocity \mathbf{v} in Equation (18)). Then f_i is also < 0 at \mathbf{r}_1 and $\mathbf{v}_2 = (v_{r2}, 0, 0)$ provided $v_{r2}^2 = v_{r1}^2 + v_{\theta1}^2 + v_{\phi1}^2$, since f_i depends on \mathbf{v} only through its modulus v . However, $f_c(\mathbf{r}_1, v_{r2}, 0, 0) = 0$ because, by definition, f_c only represents circular orbits that must have $v_r = 0$. Thus, Equation (18) shows that $f(\mathbf{r}_1, \mathbf{v}_2) < 0$ and thus is unphysical, with the only possible workaround of $\mu = 0$, and so, of all orbits being circular.

On the basis of the above arguments, ultralow-mass galaxies for which the stellar mass distribution is well fitted with cored density profiles are dynamically incompatible with an NFW profile for the dark-mass component, at least if one assumes that the phase-space DF of the stellar component depends only on the stellar energy, or that is described by an Osipkov–Merritt model, or is anisotropic with radially biased orbits, or anisotropic with tangentially biased orbits following the mixing model. These arguments cannot rule out an NFW background potential if other types of anisotropic phase-space distribution for the stars are assumed. For instance, a cored stellar profile may be compatible with a star distribution having a constant tangentially biased anisotropy (that is, having a constant and negative β). To make the range of compatibilities more clear, Table 1 lists pairs of densities and potentials together with whether they are consistent or inconsistent.

We note an important property of the consistency of a pair $\rho - \Psi$ based on whether $f(\epsilon) \geq 0 \forall \epsilon$. If a particular pair is consistent or inconsistent, then any global factor affecting the density profile will not modify this character since $f(\epsilon)$ scales linearly with a multiplicative factor in ρ (see Equations (5) and (10)). Thus, any of the inconsistencies brought out here hold true independently of the (typically unknown) mass ratio between the stars and the DM halo creating the potential.

4. Numerical Results

This section illustrates with specific examples the general results put forward in Section 3, analyzes the behavior outside the core of the system, and deals with profiles with shapes more complex than the ones considered in Section 3. We check

whether the DF resulting from particular pairs becomes negative at some point, which would discard the combination. $\beta = 0$ is assumed, so the DF $f(\epsilon)$ follows from Equations (5) and (10). Equation (5) is integrated numerically for every ϵ applying Simpson’s rule. The radial derivatives of ρ and Ψ in Equation (10) are computed analytically whenever possible using the equations in Appendix A (Section 4.1). Otherwise, we compute them numerically (Section 4.2).

4.1. Cored Density in an NFW Potential

The computation of $f(\epsilon)$ is straightforward when ρ is a Schuster–Plummer profile,

$$\rho(r) = \frac{\rho(0)}{[1 + (r/r_0)^2]^{5/2}}, \quad (29)$$

and Ψ is described by an NFW potential (Appendix A), a combination used here as a reference of cored density profile immersed in a CDM-only potential. The Schuster–Plummer profile is the polytrope of order $m = 5$, and was chosen as a reference because it provides a fair representation of the stellar mass distribution in real dwarf galaxies (e.g., Sánchez Almeida et al. 2021). As with the rest of the polytropes, this density profile has a core, therefore, it is not consistent with the potential derived from the cuspy NFW profile (Section 3). An example is shown in Figure 1. The parameters that define this polytrope and the potential have been tuned to represent a realistic galaxy with stellar mass $M_* \simeq 10^6 M_\odot$, core radius $r_0 = 1.4$ kpc, and total mass around 10^4 times the stellar mass (e.g., Behroozi et al. 2013; Kormendy & Freeman 2016). The stars are immersed in the NFW potential generated by the matter distribution represented as the gray solid line in the left panel of Figure 1. (Note that this density fully defines Ψ through Poisson’s equation and independently of the velocity distribution of the particles creating the potential.) This component completely dominates the mass and the potential of the system: the mass within the gray solid line, M_p , has $M_p/M_* \simeq 10^4$. As expected, $f < 0$ for some ϵ signaling that this combination of baryons and potential is unphysical.

For self-gravitating systems, the Poisson equation guarantees that $f(\epsilon) \geq 0 \forall \epsilon$. For the stellar density profile shown in Figure 1, $f(\epsilon)$ is analytic (Equation (A19)). We use this fact to check the numerical integration scheme used to derive $f(\epsilon)$.

4.2. Double Power-law Density and Potential

A cored density in an NFW potential is inconsistent, as we have shown. Here we expand the range of shapes to figure out how much the conditions for a core and an NFW potential can be relaxed and still become inconsistent results. In our study, we use a family of density profiles commonly used in the literature (e.g., Hernquist 1990; Merritt et al. 2006; Di Cintio et al. 2014),

$$\rho_{abc}(r) = \frac{\rho_s}{x^c (1 + x^a)^{(b-c)/a}}, \quad (30)$$

with $x = r/r_s$, that encompasses both the NFW profile ($a = 1$, $b = 3$, and $c = 1$) and the Schuster–Plummer profile ($a = 2$, $b = 5$, and $c = 0$) shown in Figure 1. Actually, for $a = 2$, $b = m$, and $c = 0$, ρ_{abc} approximately accounts for the inner region of a polytrope of index m (e.g., Sánchez Almeida 2022),

which is important in this context since polytropes describe density profiles of self-gravitating N -body systems when reaching thermodynamical equilibrium (see Plastino & Plastino 1993; Sánchez Almeida et al. 2020; Sánchez Almeida & Trujillo 2021). The constants r_s and ρ_s in Equation (30) provide the global scaling for radius and density, respectively. The parameter c gives the inner logarithmic slope

$$\lim_{r \rightarrow 0} \frac{d \log \rho_{abc}}{d \log r} = -c. \quad (31)$$

The three-parameter function ρ_{abc} can be folded into a single parameter family using $a = 2 - c$ and $b = 5 - 2c$,

$$\rho_c(r) = \frac{\rho_s}{x^c (1 + x^{2-c})^{(5-3c)/(2-c)}}, \quad (32)$$

which seamlessly scans from Schuster–Plummer to NFW when c goes from 0 to 1 (see Figure 2).

In order to compute the DF of the baryons, one needs the derivatives of the density profile and the potential (Equations (5) and (10)). Using the Poisson equation for a spherically symmetric system (e.g., An & Zhao 2013), the potential and the required derivatives can be obtained in terms of the inner mass,

$$M_p(<r) = 4\pi \int_0^r t^2 \rho_p(t) dt, \quad (33)$$

so that

$$\Psi = \frac{G M_p(<r)}{r} + 4\pi G \int_r^\infty t \rho_p(t) dt, \quad (34)$$

$$\frac{d\Psi}{dr} = -\frac{G M_p(<r)}{r^2}, \quad (35)$$

$$\frac{d^2\Psi}{dr^2} = \frac{2GM_p(<r)}{r^3} - 4\pi G \rho_p, \quad (36)$$

and

$$\frac{d^3\Psi}{dr^3} = -\frac{6GM_p(<r)}{r^4} + 8\pi G \frac{\rho_p}{r} - 4\pi G \frac{d\rho_p}{dr}, \quad (37)$$

which for $\rho_p = \rho_{abc}$ can be computed analytically only for certain values of a , b , and c (An & Zhao 2013).

Employing, Equation (30) and Equations (33)–(37), one can integrate numerically Equation (10) to obtain $f(\epsilon)$ via Equation (5). Using this approach, we have scanned through a large number of pairs of baryon densities and potentials both characterized by double exponential density profiles but with different parameters. Unless otherwise stated explicitly, we employ the simplified version of the density given in Equation (32). The main results of our numerical exercise will be discussed next and are also summarized in Table 1. To prevent confusion during the description, the parameters corresponding to the density profile that creates the potential are labeled with the subscript p whereas those of the baryon density do not have a subscript.

1. If the baryons have a core (i.e., if $c = 0$), then the density generating the potential must also have a core to be consistent (i.e., $c_p = 0$). This is shown by the numerical simulations (a counterexample with $c = 0$, $c_p = 0.05$ producing $f < 0$ is shown in Figure 3), but it also follows analytically from the study carried out in Appendix E and

discussed in item 6 below. The graphical summary in Figure 4 shows that when $c = 0$, c_p must be zero for f to be > 0 everywhere.

2. If the baryon core is not perfect ($c \gtrsim 0$; denoted as soft core in Table 1), then an NFW profile may or may not be compatible with it. Figure 5 shows examples of incompatible (top panels) and compatible (bottom panels). We have scanned a range of values for c and c_p ($-0.001 < c < 1$ and $-0.1 < c_p < 1.1$) with the compatibility summarized in Figure 4. Roughly speaking, NFW potentials ($c_p = 1$) are inconsistent with densities having $c \lesssim 0.1$.
3. Any density profile with $c = 0$ and $a > 2$ is physically unrealizable (see Figure 6), independently of the potential. The inconsistency remains even with the potential created by the self-gravity of the density and means that no $\beta = 0$ DF is able to reproduce $a > 2$ profiles. The behavior, summarized in Figure 7, is predicted analytically in Appendix E and discussed further in item 6.
4. A density profile significantly broader than the potential also yields inconsistent DFs. According to Figure 8, $r_s/r_{sp} \lesssim 2$ for the DF to be non-negative, a constraint that may be used in real galaxies to set a lower limit to the size of the DM halo from the size of the observed starlight. As we mentioned in Section 3, the density contrast between the density and the density producing the potential (ρ_s/ρ_{sp}) is irrelevant since it cannot change the sign of f .
5. Note that the region where $c > c_p$, i.e., where the baryons are cuspiers than the halo, presents no inconsistency in the summary plots of Figures 4 and 7. We bring this fact up because some numerical simulations of ultralow-mass galaxies seem to show compact stellar concentrations having $c > c_p \simeq 1$ (e.g., Orkney et al. 2021, 2023). These structures are physically feasible within the logical framework of our work which, among others, assumes negligible stellar mass ($M_* \ll M_p$) and spherical symmetry.
6. For the abc densities that we are considering, the derivative used to diagnose the positivity of the DF in Section 3 (Equation (22)) turns out to be (Equation (E3), Appendix E),

$$\frac{d\rho/dr}{d\Psi/dr} \simeq \frac{D}{r^{2+c-c_p}} \left[c + \frac{b-c}{r_s^a} r^a \right], \quad (38)$$

with $D > 0$ for $c_p < 3$. If $c \neq 0$, the first term in the RHS of Equation (38) dominates the behavior of the ratio when $r \rightarrow 0$. This term is identical to Equation (25) with $\alpha = c$ and $\alpha_p = c_p$, and to allow for the derivative to differ from zero (and so for the DF to be positive), it only demands $c > c_p - 2$. This is a very loose constraint and actually, most of the forbidden (red) region in Figures 4 and 7 actually meets this requirement. These two results, i.e., having $d\rho/d\Psi \neq 0$ and but $f < 0$ somewhere, are consistent because the first one is more demanding than the second since it requires the (weighted) integral of f to be positive (Equation (2)), which can be met even when $f < 0$ for some values of ϵ (see the example in the top panel of Figure 5). When $c = 0$, the second term in the RHS of Equation (38) rules, and then the potential and the density profiles would be inconsistent when $2 - c_p - a > 0$ since the ratio of derivatives goes to zero. For $a = 2$, as expected for polytropes, $c_p > 0$ is ruled out

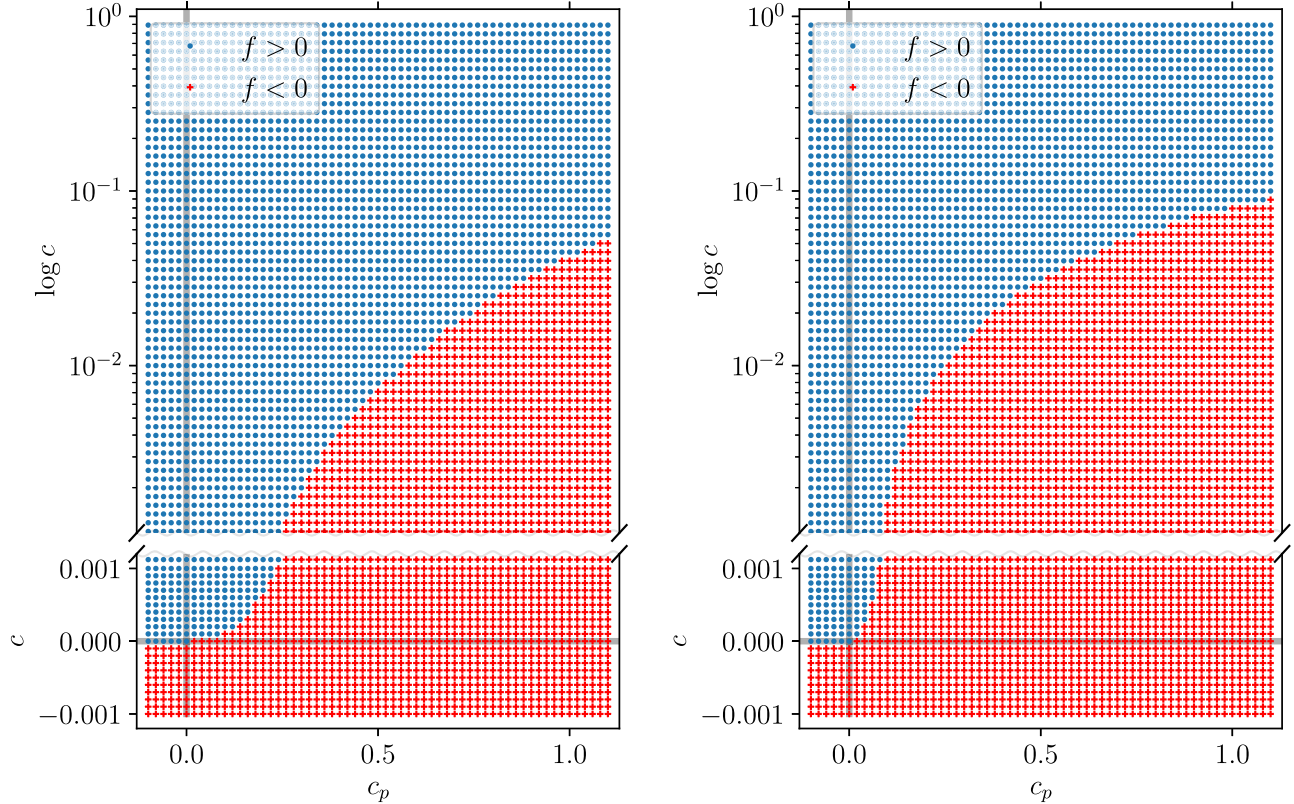


Figure 4. Summary of the allowed (blue bullet symbols) and forbidden (red plus symbols) regions of the parameter space when both the baryon density profile and the density defining the underlying potential follow a profile described by Equation (32) and illustrated in Figure 2. The symbols c and c_p represent the inner slope of the density profile and the density generating the potential, respectively. The ordinate axis is split into two (logarithmic scale on the top and linear scale at the bottom) to show the whole range of values of interest. The lines $x = 0$ and $y = 0$ are shown in light gray. Left panel: $r_s/r_{sp} = 1/4$, with the baryons more centrally concentrated than the potential. Right panel: $r_s/r_{sp} = 2$, with the baryons more spread out than the potential. Baryons do not contribute to the overall potential and their velocity distribution is assumed to be isotropic ($\beta = 0$) at all radii. In both cases, the sampling in c_p is $\Delta c_p = 0.02$ whereas the sampling in c is $\Delta c = 10^{-4}$ in the linear scale and $\Delta \log c = 0.05$ in the logarithmic scale.

and the potential must have a core to be consistent with the core in the density profile. This condition for $c = 0$ is truly restrictive, and is strictly followed by the simulations in Figure 4.

5. Discussion and Conclusions

According to the current concordance cosmological model, DM particles are collisionless, and evolving under their own gravity, produce self-gravitating structures that approximately follow the iconic NFW profile with a cusp in its center (CDM halos). These cusps ($\rho \propto r^{-1}$) are generally not observed in galaxies. The total density often presents a central plateau or core ($\rho \sim \text{const.}$), which is believed to be produced by the coupling with baryons through gravity. Star-formation-driven outbursts modify the overall gravitational potential, affecting the CDM distribution too. This mechanism of baryon feedback becomes inefficient when decreasing the galaxy’s stellar mass, reaching a point where the energy provided by baryons is simply not enough to modify the cusp of CDM halos (see Section 1 for references and details). Despite all uncertainties and model dependencies, this threshold mass roughly corresponds to isolated galaxies with stellar masses $< 10^9 M_\odot$ or halo masses $< 10^{10} M_\odot$. Thus, if these ultralow-mass galaxies show cores, they are not due to baryon feedback processes but have to reflect the nature of DM: whether it is fuzzy, self-interacting, warm, or any of the other possibilities put forward in the literature.

Direct measurements of the DM mass distribution in these faint galaxies are difficult since they require high spectral resolution spectroscopy, which is observationally extremely challenging. However, there may be a shortcut if the starlight somehow follows the DM since, even in low-mass low-luminosity galaxies, deep photometry is doable (e.g., Trujillo et al. 2021). One may naively think that stars must trace DM in these systems whose potential is fully dominated by DM. Nevertheless, stars are so weakly coupled with the DM that can potentially maintain a mass distribution differing from the DM distribution for longer than the age of the Universe (e.g., Binney & Tremaine 2008). Thus, in order to use the observable stellar mass distribution as a proxy for the elusive DM distribution, one has to show that somehow starlight traces DM in these DM-dominated systems. More specifically, we know that low-mass galaxies often show cores in their stellar mass distribution (Section 1). The question arises as to whether or not this cored baryon distribution is consistent with the DM distribution expected from CDM particles (a.k.a. NFW profile). We address the question using the so-called Eddington inversion method. Under mildly restrictive assumptions (gravity from baryons negligible, stationary state, smooth potential, and spherical symmetry; see Section 2), the method provides the DF in the phase-space f corresponding to a mass density distribution immersed in a gravitational potential. Given two arbitrary densities and potentials, there is no guarantee that $f > 0$ everywhere, which is required for them to be physically consistent.

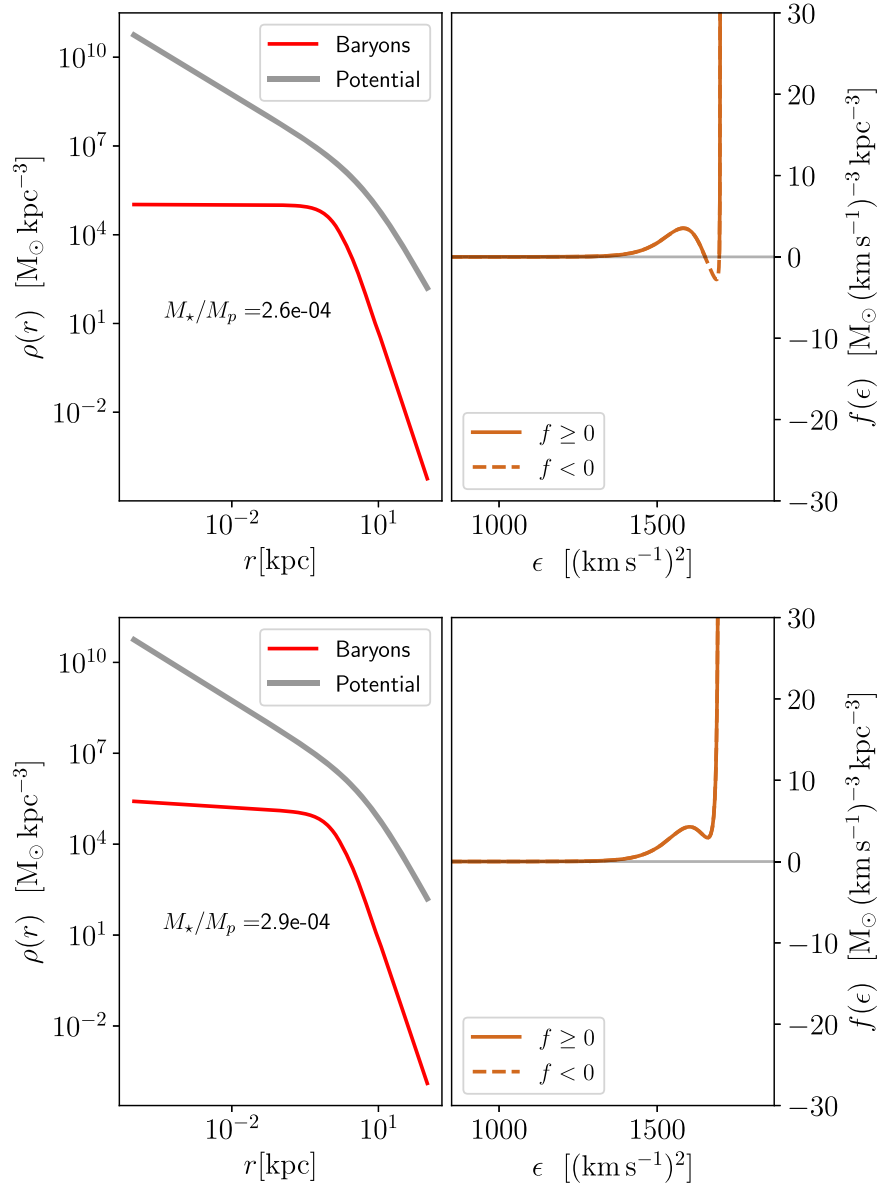


Figure 5. Top panels: similar to Figure 1 but with a hint of cusp in the density: $c = 0.005$ and $c_p = 1$. The DF $f < 0$ but not at the largest ϵ . This combination of the baryon soft core and NFW potential is still inconsistent. However, the inconsistency goes away as soon as the inner slope of the stellar density profile increases, as shown in the bottom panels, where $c = 0.1$ and $c_p = 1$. The global picture of compatibility–incompatibility is summarized in Figure 4. The shape of the profiles defining the baryon distribution and the potential is given by Equation (32).

In this paper, we have studied different combinations of baryon density and gravitational potential that may help us to discern whether or not DM profiles in ultralow-mass galaxies have a core. We focus on the consistency of the various gravitational potentials with baryon density profiles showing a core (Equation (23)) or soft core (Equation (31), with $c \gtrsim 0$). The main conclusions of our analysis are summarized in Table 1 and can be expanded as follows:

1. Stellar cores in a NFW potential are incompatible provided the velocity distribution is isotropic ($\beta = 0$).
2. Stellar cores and potentials stemming from a density with a quasi-core ($c_p > 0$) are incompatible too. This result holds for isotropic velocities ($\beta = 0$).
3. As expected for physical consistency, stellar cores and potentials resulting from cored density profiles are

consistent in isotropic ($\beta = 0$) and radially biased systems ($\beta > 0$).

4. Stellar cores and NFW potentials are also incompatible in systems with anisotropic velocities provided they follow the Osipkov–Merritt model. Even if artificial, it approximately describes the global trend expected in ultralow-mass galaxies, with $\beta \sim 0$ in the center and then increasing outward ($\beta > 0$).
5. Stellar cores and NFW potentials are incompatible in systems with radially biased orbits (const. $\beta > 0$). Actually, a stellar core is incompatible with any potential without a core in systems with constant radially biased orbits ($\beta > 0$).
6. Circular orbits ($\beta = -\infty$) can accommodate any combination of baryon density and potential, including a cored stellar density in an NFW potential. This configuration is

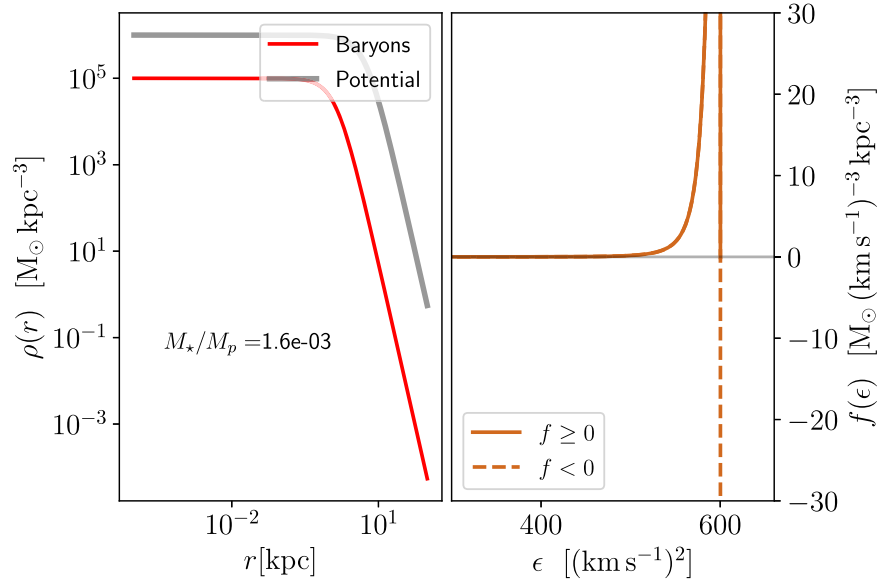


Figure 6. Similar to Figure 5 with $c = c_p = 0$ and $a = a_p = 2.1$. Even if the two density profiles have the same shape, $f < 0$ somewhere (the dashed line). This behavior for $a > 2$ is predicted analytically in Appendix E and discussed further in Section 4.2, item 6.

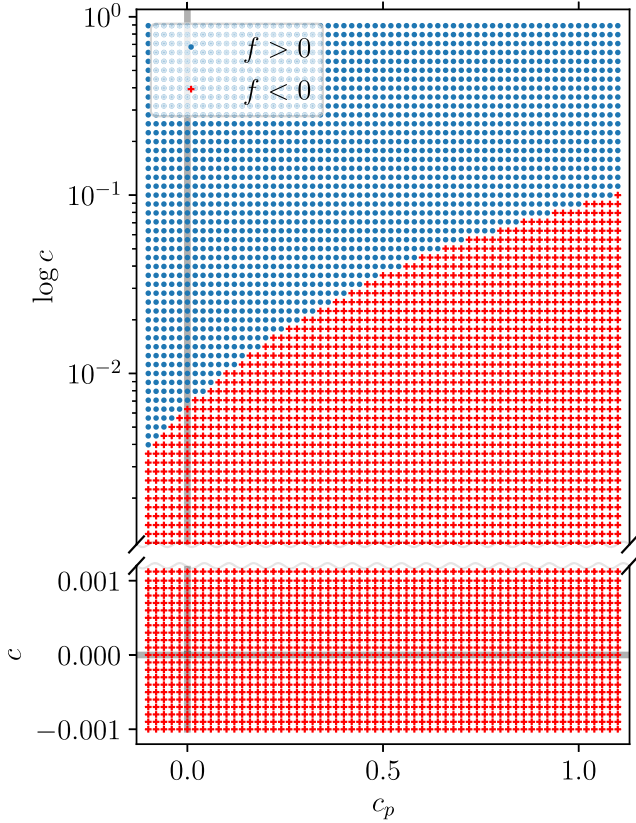


Figure 7. Similar to Figure 4 but using $a = 2.5 - c$, so that Equation (38) (or Equation (E4)) can be tested. Note that $c = c_p = 0$ is unphysical even though ρ and the density profile producing the potential are identical.

very artificial, though, and unlikely to happen in real dwarf galaxies where orbits are expected to be radially biased (see the discussion below).

7. The linear superposition of two DFs is also a DF. Thus, one may think that the addition of a positive DF for circular orbits may compensate for the negative DF for isotropic orbits to yield a positive physically sensible DF.

However, this is not the case. Independently of the relative weight, the mixing of an unphysical DF for isotropic velocities ($\beta = 0$) with a physically realizable DF for circular orbits ($\beta = -\infty$) always yields unphysical DFs (Section 2.3).

8. We denote as soft cores zero but close to it ($c \gtrsim 0$). Soft cores are inconsistent with NFW profiles when $c \lesssim 0.1$ while they are consistent when $c \gtrsim 0.1$. When the density profile that characterizes the potential also has a soft core (i.e., when $0 \leq c_p \leq 1$), then the situation is more complicated as shown in, e.g., Figure 4. This statement holds for isotropic velocity distributions.
9. The inner slope of a soft stellar core and the radial anisotropy are related so that $c > 2\beta$. In other words, large radially biased orbits are strongly inconsistent with soft stellar cores.
10. Positive inner slope in the stellar distribution, where the density grows outward, is discarded in every way.
11. For stellar densities and potentials with the same shape (whether cored or not), the stellar density distribution cannot be broader than twice the width of the density equivalent to the potential. This result refers to isotropic velocities and may be used in real galaxies to set a lower limit to the size of the DM halo from the size of the observed starlight.
12. Pairs of density and potential where the inner slope of the density is larger than that of the potential ($c \geq c_p$) are not inconsistent. This result refers to isotropic velocities too.
13. The above conclusions do not depend on a scaling factor on the stellar density profile, therefore, they do not depend on the (unknown) ratio between the stellar mass and the total mass of the system.
14. The functions used to represent the density and the potential are flexible enough to describe the central region in any polytrope of arbitrary index m (Equation (30), with $a = 2$, $b = m$, and $c = 0$). Polytropes are important in the context of self-gravitating systems since they describe the density expected in N -body systems reaching

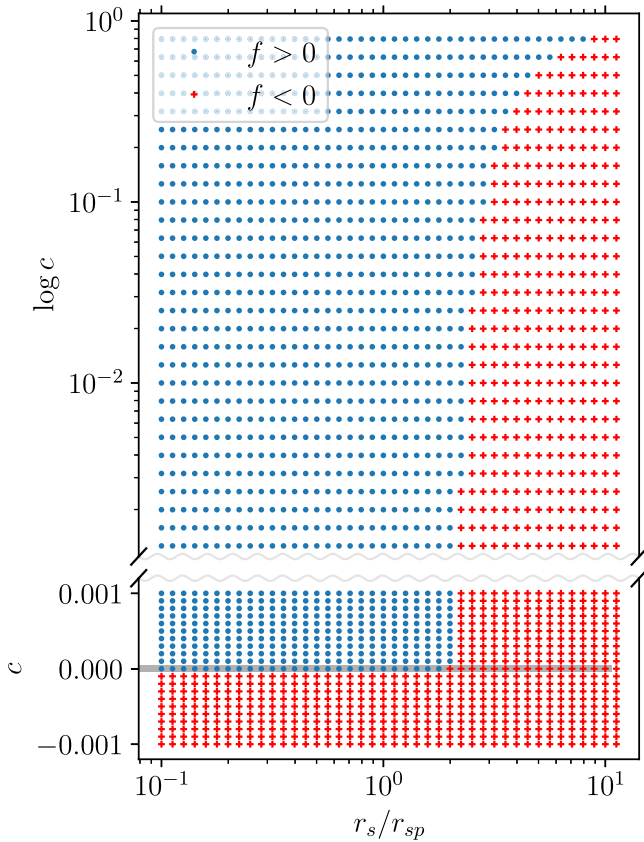


Figure 8. Diagnostic plot similar to that in Figure 4, except that this time we represent simulations where both c and r_s/r_{sp} are varied. Note how r_s cannot be larger than $\sim 2 r_{sp}$ for f to remain positive, a constraint that may be used in real galaxies to set a lower limit to the size of the DM halo. In these simulations the abc profile shapes of density and potential are identical, explicitly, $a = a_p$, $b = b_p$, and $c = c_p$, the three of them varying as for Equation (32). The sampling in c is $\Delta c = 10^{-4}$ in the linear scale and $\Delta \log c = 0.1$ in the logarithmic scale. The relative radii are shown in a logarithmic scale with a sampling of $\Delta \log(r_s/r_{sp}) = 0.1$.

thermodynamical equilibrium (see Plastino & Plastino 1993; Sánchez Almeida et al. 2020). In other words, they portray the DM density distribution expected if the DM were not collisionless (e.g., Sánchez Almeida & Trujillo 2021).

How useful the above constraints are very much depends on the anisotropy of the velocity field β (Equation (11)). In general, radially biased ($\beta > 0$) and isotropic ($\beta = 0$) orbits are more difficult to reconcile with a cuspy gravitational potential than tangentially biased orbits ($\beta < 0$). The question arises as to what anisotropy is to be expected in real galaxies. This issue can be addressed from two complementary directions, namely, what is the anisotropy observed in the smallest galaxies, and what is the anisotropy recovered for the smallest galaxies formed in cosmological numerical simulations. Even if the uncertainties are large because the estimates rely on measuring velocities of individual stars, the DM-dominated satellites of the MW tend to have $\beta \gtrsim 0$ (e.g., Łokas 2009; Massari et al. 2018; Read et al. 2019; Massari et al. 2020; Leung et al. 2021; Kowalczyk & Łokas 2022). Note that these objects are not isolated galaxies and their internal baryon structure may be strongly mediated by the presence of the MW and its circumgalactic medium through tidal forces, ram pressure, and starvation (e.g., Combes 2004; Benson 2010; Sánchez

Almeida et al. 2017). However, the observed trend is consistent with numerical simulations. Radial anisotropies seem to be the natural outcome of the formation of dwarf galaxies in Λ CDM cosmological numerical simulations: see, e.g., El-Badry et al. (2017), Figure 2, and Orkney et al. (2023), Figure 5. Moreover, β tends to zero when approaching the center of the gravitational potential, where the stellar cores may be present and have to be observed. Thus, $\beta \gtrsim 0$ at the centers seems to be a sensible conjecture when interpreting stellar mass distributions in real galaxies.

One of the seemingly more restrictive assumptions leading to the constraints in Table 1 is the spherical symmetry of the density and potential. As it happens with the isotropy of the velocity field, the question of whether this is a good assumption for real ultralow-mass galaxies arises. Actually, the two issues are closely connected since, in real galaxies, both are set by the history of star formation driven by cosmological gas accretion and mergers (e.g., Dekel et al. 2009; Sánchez Almeida et al. 2014). In general, the smallest simulated galaxies tend to be rounded, although not perfectly spherical, with the DM component closer to sphericity (e.g., Bullock 2002; Orkney et al. 2023). On the other hand, the observed dwarf isolated galaxies are triaxial, but with three axes of similar lengths (e.g., Roychowdhury et al. 2013; Sánchez-Janssen et al. 2016; Putko et al. 2019). In addition to whether or not real ultralow-mass galaxies are well fitted by spherically symmetric models, independent theoretical arguments point out that this assumption is not so critical since the incompatibilities may still hold when dropped. The extensions of the Eddington inversion method for axisymmetric systems (Lynden-Bell 1962; Binney & Tremaine 2008) lead to expressions for the DF similar to Equations (2), (15), and (D3). They are expected to lead to restrictions similar to those worked out in this paper. We are presently exploring them with promising results. There are also extensions or variants of the Eddington inversion approach, suitable for other more general spherically symmetric DFs, that in principle could be used for diagnostics and would be worth considering (e.g., Dejonghe 1987; Cuddeford 1991; Strigari et al. 2017), but their analysis remains to be carried out.

The constraints in Table 1 result from treating particular cases, each one with its own peculiarities. The analysis of other cases (e.g., the study of axisymmetric systems mentioned above) will enlarge a list that at present contains only a fraction of the constraints yet to be discovered. In this sense, our work is only a pathfinder that shows how the traditional Eddington method can be used to study DM halos in ultralow-mass galaxies. Given the observed stellar distribution, the method seriously limits the properties of the DM halo where it resides. Moreover, its interest probably exceeds the original scope that motivated the present study, and may be of application to other astrophysical systems where the stars represent only a minor fraction of the total mass, for example, the intra-cluster light as a tracer of the DM galaxy cluster potential (e.g., Montes & Trujillo 2019, 2022).

In short, the question in the title of the paper, Can CDM matter halos hold cored stellar mass distributions? has no simple yes or no answer. Instead, we find it to be unlikely, although not impossible, that cored stellar mass distributions can be hosted in NFW DM halos, provided the system is spherically symmetric. Thus, our work supports the interest in determining surface brightness profiles of ultralow-mass galaxies to constrain the nature of DM. This work can be used

as a guide to interpreting observations so that the closer the observed galaxies are to the hypotheses (spherically symmetry, stationarity, velocity isotropy, etc.), the more useful the constraints in Table 1.

Our ultimate goal is to apply the mathematical tools developed in this paper to the observed dwarf galaxies with masses low enough to constrain the nature of DM (Section 1). This challenging task still requires several intermediate steps to be completed. In our roadmap, we would like to test the machinery with the few Local Group galaxies for which independent information on the DM halo and on the stellar distribution is available (e.g., Battaglia & Nipoti 2022), to see whether the constraints imposed by the Eddington inversion method and by the kinematical measurements are consistent. We also need to know what is the signal-to-noise ratio and the number of targets required to make firm claims. Having 100 targets with surface brightness profiles reaching down to 30 mag arcsec⁻² seems to be doable (e.g., Carlsten et al. 2021) but, does it suffice? Finally, we have to carefully select the actual data set of faint isolated dwarf galaxies. The two requirements are in tension since intrinsically faint galaxies are nearby and so tend to be satellites, but both are needed. One obvious possibility is waiting for better data (e.g., Ivezić et al. 2019; Abbott et al. 2021; Trujillo et al. 2021). Alternatively, one can also think of studying the ultra-faint dwarfs of the Local Group (e.g., Moskowit & Walker 2020) cherry-picking those where the tidal forces and other environmental effects may be minimal (e.g., with large pericentric passage) and which truly proceed from low-mass progenitors (e.g., Grebel et al. 1926). Tidal forces change the internal structure of satellites and reduce their stellar mass content, thus blurring any clear-cut interpretation of the observed DM distribution in terms of the nature of DM, a caveat to keep in mind if this pathway is chosen. All these works are currently ongoing or planned.

Acknowledgments

Thanks are due to Claudio Dalla-Vechhia for insightful discussions during the early stages of the work, and to Giuseppina Battaglia, Arianna Di Cintio, and Ruben Sánchez-Janssen for references. Thanks are due to Matthew Orkney and Justin Read for discussions and clarifications on the velocity anisotropy and mass profile of the galaxies in their simulations. J.S.A. acknowledges financial support from the Spanish Ministry of Science and Innovation (MICINN), projects PID2019-107408GB-C43 and PID2022-136598NB-C31 (ESTALLIDOS). J.S.A.'s visit to La Plata was partly covered by the MICINN through the Spanish State Research Agency, under the Severo Ochoa Centers of Excellence Programme 2020-2023 (CEX2019-000920-S). J.S.A. also wants to explicitly thank Angel Luis Platino and the Facultad de Ciencias Económicas de La Universidad Nacional de La Plata for their hospitality during this visit. A.R.P. acknowledges support to visit the IAC from the Fundación Jesús Serra and the IAC under their Visiting Researcher Programme 2020–2022. I.T. acknowledges support from Project PCI2021-122072-2B, financed by MICIN/AEI/10.13039/501100011033, and the European Union NextGenerationEU/RTRP and the ACIISI, Consejería de Economía, Conocimiento y Empleo del Gobierno de Canarias and the European Regional Development Fund (ERDF) under grant No. PROID2021010044 and from the State Research Agency (AEI-MCINN) of the Spanish

Ministry of Science and Innovation under grant No. PID2019-107427GB-C32 and IAC project P/302302, financed by the Ministry of Science and Innovation, through the State Budget and by the Canary Islands Department of Economy, Knowledge, and Employment, through the Regional Budget of the Autonomous Community.

Software: NumPy (Harris et al. 2020), SciPy (Virtanen et al. 2020).

Appendix A

Analytic Derivatives of the Density and the Potential

According to Equations (5) and (10), the DF $f(\epsilon)$ corresponding to a density $\rho(r)$ in a potential $\Psi(r)$ can be deduced from the first three derivatives of $\rho(r)$ and $\Psi(r)$. This appendix works them out for various practical cases that involve polytropes and NFW potentials. They all are used in the main text.

A.1. DF for a Schuster–Plummer Stellar Mass Density in an NFW Potential

The Schuster–Plummer density (Equation (29)) is defined as

$$D(r) = \rho(0) \left[1 + \frac{r^2}{r_0^2} \right]^{-\frac{5}{2}}, \quad (\text{A1})$$

so that

$$\frac{dD}{dr} = D_1(r) = -\frac{5\rho(0)}{r_0^2} r \left[1 + \frac{r^2}{r_0^2} \right]^{-\frac{7}{2}}, \quad (\text{A2})$$

$$\begin{aligned} \frac{d^2D}{dr^2} = D_2(r) = & -\frac{5\rho(0)}{r_0^2} \left[1 + \frac{r^2}{r_0^2} \right]^{-\frac{7}{2}} \\ & + \frac{35\rho(0)}{r_0^4} r^2 \left[1 + \frac{r^2}{r_0^2} \right]^{-\frac{9}{2}}, \end{aligned} \quad (\text{A3})$$

and

$$\begin{aligned} \frac{d^3D}{dr^3} = D_3(r) = & \frac{35\rho(0)}{r_0^4} r \left[1 + \frac{r^2}{r_0^2} \right]^{-\frac{9}{2}} + \frac{70\rho(0)}{r_0^4} r \\ & + \left[1 + \frac{r^2}{r_0^2} \right]^{-\frac{9}{2}} - \frac{315\rho(0)}{r_0^6} r^3 \left[1 + \frac{r^2}{r_0^2} \right]^{-\frac{11}{2}}. \end{aligned} \quad (\text{A4})$$

On the other hand, the NFW density profile is defined as

$$\rho_{\text{NFW}}(r) = \frac{\rho_s}{(r/r_s)(1+r/r_s)^2}, \quad (\text{A5})$$

with r_s and ρ_s two constants. It creates a potential given by (e.g., Binney & Tremaine 2008),

$$\Phi_{\text{NFW}}(r) = -\frac{V_c}{r} \ln \left(1 + \frac{r}{r_s} \right), \quad (\text{A6})$$

with $V_c = 4\pi G \rho_s r_s^3$. Then the relative potential $\Psi(r)$, denoted for the NFW profile as $V(r)$, turns out to be

$$V(r) = \Phi_{\text{NFW}}(\infty) - \Phi_{\text{NFW}}(r) = \frac{V_c}{r} \ln \left(1 + \frac{r}{r_s} \right), \quad (\text{A7})$$

with its derivatives given by

$$\frac{dV}{dr} = V_1(r) = \frac{V_c}{r^2} \left[\frac{r}{r+r_s} - \ln \left(1 + \frac{r}{r_s} \right) \right], \quad (\text{A8})$$

$$\frac{d^2V}{dr^2} = V_2(r) = -\frac{2V_c}{r^3} \left[\frac{r}{r+r_s} - \ln \left(1 + \frac{r}{r_s} \right) \right] - \frac{V_c}{r(r+r_s)^2}, \quad (\text{A9})$$

and

$$\begin{aligned} \frac{d^3V}{dr^3} = V_3(r) &= \frac{6V_c}{r^4} \left[\frac{r}{r+r_s} - \ln \left(1 + \frac{r}{r_s} \right) \right] \\ &+ \frac{2V_c}{r^2(r+r_s)^2} + \frac{V_c(3r+r_s)}{r^2(r+r_s)^3}. \end{aligned} \quad (\text{A10})$$

Using Equations (5) and (10), the DF corresponding to a density given by Equation (A1) and a potential set by Equation (A7) turns out to be

$$\begin{aligned} f(\epsilon) &= \frac{1}{\pi^2 \sqrt{2}} \int_R^\infty dr \sqrt{\epsilon - V(r)} \\ &\left[\frac{-D_3}{V_1^2} + \frac{3D_2V_2}{V_1^3} + \frac{D_1V_3}{V_1^3} - \frac{3D_1V_2^2}{V_1^4} \right], \end{aligned} \quad (\text{A11})$$

with the limit R implicitly defined as $\epsilon = V(R)$.

A.2. Distribution Function for a Schuster–Plummer Stellar Mass Density in a Schuster–Plummer Potential

The gravitational potential corresponding to the mass density in Equation (A1) is (e.g., Binney & Tremaine 2008)

$$\Phi_{\text{SP}}(r) = -W_c \left(1 + \frac{r^2}{r_0^2} \right)^{-1/2}, \quad (\text{A12})$$

with

$$W_c = \rho(0) \left(\frac{4\pi}{3} \right) G r_0^2 \quad (\text{A13})$$

so that the corresponding relative potential becomes

$$W(r) = \Phi_{\text{SP}}(\infty) - \Phi_{\text{SP}}(r) = W_c \left(1 + \frac{r^2}{r_0^2} \right)^{-1/2}, \quad (\text{A14})$$

with its derivatives given by

$$\frac{dW}{dr} = W_1(r) = -\frac{W_c}{r_0^2} r \left(1 + \frac{r^2}{r_0^2} \right)^{-3/2}, \quad (\text{A15})$$

$$\begin{aligned} \frac{d^2W}{dr^2} = W_2(r) &= -\frac{W_c}{r_0^2} \left(1 + \frac{r^2}{r_0^2} \right)^{-3/2} \\ &+ \frac{3W_c}{r_0^4} r^2 \left(1 + \frac{r^2}{r_0^2} \right)^{-5/2}, \end{aligned} \quad (\text{A16})$$

and

$$\begin{aligned} \frac{d^3W}{dr^3} = W_3(r) &= \frac{9W_c}{r_0^4} r \left(1 + \frac{r^2}{r_0^2} \right)^{-5/2} \\ &- \frac{15W_c}{r_0^6} r^3 \left(1 + \frac{r^2}{r_0^2} \right)^{-7/2}. \end{aligned} \quad (\text{A17})$$

Using Equations (5) and (10), the DF corresponding to a density given by Equation (A1) and a potential set by Equation (A14) turns out to be

$$\begin{aligned} f(\epsilon) &= \frac{1}{\pi^2 \sqrt{2}} \int_R^\infty dr \sqrt{\epsilon - W(r)} \\ &\left[\frac{-D_3}{W_1^2} + \frac{3D_2W_2}{W_1^3} + \frac{D_1W_3}{W_1^3} - \frac{3D_1W_2^2}{W_1^4} \right], \end{aligned} \quad (\text{A18})$$

with the radius R implicitly defined as $\epsilon = W(R)$. In the case of a self-gravitating system, so that the Schuster–Plummer potential is the one created by the Schuster–Plummer mass density, then Equation (A18) can be integrated analytically to yield

$$f(\epsilon) = \frac{\rho(0)}{W_c^5} \frac{120}{(2\pi)^{3/2} \Gamma(9/2)} \epsilon^{7/2}, \quad (\text{A19})$$

an expression used to check our numerical evaluations of $f(\epsilon)$.

Appendix B

The Terms at $\Psi = 0$ in the Eddington Inversion Method

The relative potential Ψ generated by a spherically symmetric system of finite total mass behaves as $\Psi \propto r^{-1}$ for $r \rightarrow \infty$ (e.g., Equation (34)). Consider objects where $\rho \propto r^{-b}$ for $r \rightarrow \infty$ (e.g., Equation (30)). Combining the asymptotic behaviors of Ψ and ρ , one finds that $d\rho/d\Psi \propto r^{1-b}$ and $d^2\rho/d\Psi^2 \propto r^{2-b}$. Consequently, $(d\rho/d\Psi)_{\Psi=0} = (d^2\rho/d\Psi^2)_{\Psi=0} = 0$ provided $b > 2$. The above argument is not strictly valid if Ψ stands for the NFW potential because it does not correspond to a mass distribution with finite total mass, and it behaves as $\Psi \propto r^{-1} \ln r$ for $r \rightarrow \infty$. However, if $b > 2$, using Equation (7), one can show that $(d\rho/d\Psi)_{\Psi=0} = (d^2\rho/d\Psi^2)_{\Psi=0} = 0$ still when $r \rightarrow \infty$, in spite of the logarithmic factor appearing in the NFW potential.

Appendix C

DF of a Spherically Symmetric System with Circular Orbits

Any density $\rho(r)$ can be reproduced with a system of spherically symmetric circular orbits (Binney & Tremaine 2008, Section 4.3.2). By definition, their radial velocity is zero, $v_r = 0$, and their tangential velocity is equal to the circular velocity, $v_t = v_c(r)$, with

$$v_c^2(r) = \frac{G M_p(<r)}{r}. \quad (\text{C1})$$

The symbol $M_p(<r)$ stands for the inner mass creating the potential Φ . A general DF with the required properties is

$$f_c(r, v_t, v_r) = F(r) \delta(v_t - v_c) \delta(v_r), \quad (\text{C2})$$

where δ represents a Dirac-delta function and F is a function to be set by the density. Since ρ is recovered from the integral of

f_c over all velocities,

$$\rho(r) = 2\pi \iint f_c v_t dv_t dv_r, \quad (\text{C3})$$

then

$$F(r) = \frac{\rho(r)}{2\pi v_c(r)}, \quad (\text{C4})$$

which, together with Equation (C1), uniquely defines F for any combination of ρ and Φ . Note that even if the DF in Equation (C2) is not explicitly written in terms of ϵ and L , it is straightforward to verify that it is a stationary DF.

Appendix D

The Theorem by An & Evans (2006) in Our Context

Section 2.4 puts forward the DF,

$$f(\epsilon, L) = L^{-2\beta} f_\epsilon(\epsilon), \quad (\text{D1})$$

which represents a leading order approximation for a wide class of DFs having the anisotropy parameter β constant (An & Evans 2006; Binney & Tremaine 2008). In this case, the DF depends not only on the energy ϵ but also on the modulus of the angular momentum L . Under this assumption, the mass volume density can be written as (Binney & Tremaine 2008, Equation (4.66)),

$$r^{2\beta} \rho(r) = \kappa_\beta \int_0^\Psi \frac{f_\epsilon(\epsilon)}{(\Psi - \epsilon)^{\beta-1/2}} d\epsilon, \quad (\text{D2})$$

where κ_β is a positive numerical value independent of the radius r . As we argued in Section 3, for the integral in the RHS of Equation (D2) to be zero, $f_\epsilon < 0$ somewhere which through Equation (D1) makes f unphysical. Assuming $\rho(r) \propto r^{-\alpha}$ when $r \rightarrow 0$, then the left-hand-side of Equation (D2) differs from zero if $2\beta - \alpha \leq 0$, which is the theorem proved by An & Evans 2006. Here we go a step further and provided $\beta < 1/2$ (Equation (D2) diverges when taking derivatives and $\beta > 1/2$), one obtains (Binney & Tremaine 2008 Equation (4.67)),

$$\frac{d[r^{2\beta} \rho(r)]/dr}{d\Psi/dr} = \kappa_\beta \left(\frac{1}{2} - \beta \right) \int_0^\Psi \frac{f_\epsilon(\epsilon)}{(\Psi - \epsilon)^{\beta+1/2}} d\epsilon. \quad (\text{D3})$$

In the case of Ψ given by an NFW potential, its radial derivative at $r=0$ differs from zero and is negative (Equation (24)) therefore, to avoid the RHS of Equation (D3) to be less or equal to zero (and so to avoid an unphysical $f_\epsilon < 0$), $2\beta - \alpha \neq 0$ and $2\beta - \alpha - 1 \leq 0$. The second condition is automatically met because $2\beta - \alpha$ is already ≤ 0 according to An & Evans (2006). Together with this inequality, the first condition implies that for $f > 0$ then

$$\alpha > 2\beta. \quad (\text{D4})$$

Our derivation assumes $\beta < 1/2$, however, it is not difficult to show that the inequality still holds in the limit case when $\beta = 1/2$ and Equation (D3) is not valid.

There are several obvious consequences of the inequality in Equation (D4): (1) cores ($\alpha = 0$) are inconsistent with isotropic velocities ($\beta = 0$), (2) cores are inconsistent with radially biased velocities (i.e., only $\beta < 0$ is allowed), (3) radially biased orbits ($0 < \beta < 1/2$) require cuspy baryon density

profiles ($\alpha > 0$), and (4) circular orbits do not pose any problem since $\beta = -\infty$.

Appendix E

Value of $(d\rho/dr)/(d\Psi/dr)$ when $r \rightarrow 0$ and $d\rho/dr \rightarrow 0$

Starting out from the definition of ρ_{abc} in Equation (30), one finds for $r \rightarrow 0$,

$$\frac{d\rho_{abc}}{dr} \simeq -\frac{\rho_s}{r_s} \frac{c + (b-c)x^a}{x^{1+c}}, \quad (\text{E1})$$

with $x = r/r_s$. Similarly, Equation (35) provides the first-order approximation,

$$\frac{d\Psi}{dr} \simeq -B r^{1-c_p}, \quad (\text{E2})$$

where c_p is the value of c of the density profile assumed to generate the potential Ψ and B is a positive constant. Putting together the two previous equations, one finds

$$\frac{d\rho/dr}{d\Psi/dr} \simeq \frac{D}{r^{2+c-c_p}} \left[c + \frac{b-c}{r_s^a} r^a \right], \quad (\text{E3})$$

with $D > 0$ for $c_p < 3$. In the range of interest for galaxies, the parameters c and c_p are from ~ 0 to ~ 1 , with $c \leq c_p$, whereas a is between ~ 1 and ~ 2 . If $c \neq 0$, the first term on the RHS of Equation (E3) dominates the behavior of the ratio when $r \rightarrow 0$. This term is identical to Equation (25) with $\alpha = c$ and $\alpha_p = c_p$, and its behavior is discussed in detail in Section 3. The case when $c = 0$ is particularly interesting since it represents a cored density profile. Only the second term on the RHS of Equation (E3) is not zero and it turns out to be

$$\frac{d\rho/dr}{d\Psi/dr} \simeq \frac{D b}{r_s^a} \frac{1}{r^{2-c_p-a}}. \quad (\text{E4})$$

Thus, the potential and the density profiles would be inconsistent when $2 - c_p - a < 0$ since the ratio of derivatives goes to zero when $r \rightarrow 0$. It implies that when $a = 2$ (e.g., Schuster–Plummer profile; Appendix A.2), all $c_p > 0$ are physically unrealizable (see Figure 4 for $c = 0$). It also implies that when $c_p = 0$, and so the potential has the same core as the density, the pair density and potential are unphysical for $a > 2$. This somewhat surprising behavior has been checked numerically (Figures 6 and 7).

ORCID iDs

Jorge Sánchez Almeida  <https://orcid.org/0000-0003-1123-6003>

Angel R. Plastino  <https://orcid.org/0000-0001-5848-0770>

Ignacio Trujillo  <https://orcid.org/0000-0001-8647-2874>

References

- Abbott, T. M. C., Adamów, M., Aguena, M., et al. 2021, *ApJS*, 255, 20
 An, J., & Zhao, H. 2013, *MNRAS*, 428, 2805
 An, J. H., & Evans, N. W. 2006, *ApJ*, 642, 752
 Battaglia, G., & Nipoti, C. 2022, *NatAs*, 6, 659
 Bechtol, K., Birrer, S., Cyr-Racine, F.-Y., et al. 2022, arXiv:2203.07354
 Behroozi, P. S., Wechsler, R. H., & Conroy, C. 2013, *ApJ*, 770, 57
 Benson, A. J. 2010, *PhR*, 495, 33
 Binney, J., & Tremaine, S. 2008, *Galactic Dynamics* (2nd edn.; Princeton, NJ: Princeton Univ. Press)

- Blumenthal, G. R., Faber, S. M., Primack, J. R., & Rees, M. J. 1984, *Natur*, **311**, 517
- Breddels, M. A., & Helmi, A. 2013, *A&A*, **558**, L3
- Brown, S. T., McCarthy, I. G., Diemer, B., et al. 2020, *MNRAS*, **495**, 4994
- Bullock, J. S. 2002, in Proc. of the Yale Cosmology Workshop, The Shapes of Galaxies and Their Dark Halos, ed. P. Natarajan (Singapore: World Scientific), 109
- Bullock, J. S., & Boylan-Kolchin, M. 2017, *ARA&A*, **55**, 343
- Carlsten, S. G., Greene, J. E., Greco, J. P., Beaton, R. L., & Kado-Fong, E. 2021, *ApJ*, **922**, 267
- Cen, R. 2014, *ApJL*, **790**, L24
- Chan, T. K., Kereš, D., Oñorbe, J., et al. 2015, *MNRAS*, **454**, 2981
- Ciotti, L. 1996, *ApJ*, **471**, 68
- Ciotti, L., & Pellegrini, S. 1992, *MNRAS*, **255**, 561
- Combes, F. 2004, in IAU Symp. 217, Recycling Intergalactic and Interstellar Matter, ed. P.-A. Duc, J. Braine, & E. Brinks (San Francisco, CA: ASP), 440
- Cuddeford, P. 1991, *MNRAS*, **253**, 414
- Davis, M., Efstathiou, G., Frenk, C. S., & White, S. D. M. 1985, *ApJ*, **292**, 371
- Davis, M., Efstathiou, G., Frenk, C. S., & White, S. D. M. 1992, *Natur*, **356**, 489
- Dejonghe, H. 1987, *MNRAS*, **224**, 13
- Dekel, A., Birnboim, Y., Engel, G., et al. 2009, *Natur*, **457**, 451
- Del Popolo, A., & Le Delliou, M. 2017, *Galax*, **5**, 17
- Di Cintio, A., Brook, C. B., Dutton, A. A., et al. 2014a, *MNRAS*, **441**, 2986
- Di Cintio, A., Brook, C. B., Macciò, A. V., et al. 2014b, *MNRAS*, **437**, 415
- Dodelson, S., & Widrow, L. M. 1994, *PhRvL*, **72**, 17
- Eddington, A. S. 1916, *MNRAS*, **76**, 572
- El-Badry, K., Wetzel, A. R., Geha, M., et al. 2017, *ApJ*, **835**, 193
- Expósito-Márquez, J., Brook, C. B., Huertas-Company, M., et al. 2023, *MNRAS*, **519**, 4384
- Governato, F., Brook, C., Mayer, L., et al. 2010, *Natur*, **463**, 203
- Grebel, E. K., Gallagher, J. S. I., & Harbeck, D. 2003, *AJ*, **125**, 1926
- Harris, C. R., Millman, K. J., van der Walt, S. J., et al. 2020, *Natur*, **585**, 357
- Hayashi, K., Chiba, M., & Ishiyama, T. 2020, *ApJ*, **904**, 45
- Hernquist, L. 1990, *ApJ*, **356**, 359
- Hu, W., Barkana, R., & Gruzinov, A. 2000, *PhRvL*, **85**, 1158
- Ivezić, Ž., Kahn, S. M., Tyson, J. A., et al. 2019, *ApJ*, **873**, 111
- Jackson, R. A., Martin, G., Kaviraj, S., et al. 2021, *MNRAS*, **502**, 4262
- Kormendy, J., & Freeman, K. C. 2016, *ApJ*, **817**, 84
- Kowalczyk, K., & Łokas, E. L. 2022, *A&A*, **659**, A119
- Lacroix, T., Stref, M., & Lavalley, J. 2018, *JCAP*, **2018**, 040
- Leung, G. Y. C., Leaman, R., Battaglia, G., et al. 2021, *MNRAS*, **500**, 410
- Łokas, E. L. 2009, *MNRAS: Lett.*, **394**, L102
- Lotz, J. M., Jonsson, P., Cox, T. J., & Primack, J. R. 2008, *MNRAS*, **391**, 1137
- Lynden-Bell, D. 1962, *MNRAS*, **123**, 447
- Oñorbe, J., Breddels, M. A., Helmi, A., et al. 2018, *NatAs*, **2**, 156
- Massari, D., Helmi, A., Mucciarelli, A., et al. 2020, *A&A*, **633**, A36
- Merritt, D., Graham, A. W., Moore, B., Diemand, J., & Terzić, B. 2006, *AJ*, **132**, 2685
- Montes, M., & Trujillo, I. 2019, *MNRAS*, **482**, 2838
- Montes, M., & Trujillo, I. 2022, *ApJL*, **940**, L51
- Moskowitz, A. G., & Walker, M. G. 2020, *ApJ*, **892**, 27
- Navarro, J. F., Frenk, C. S., & White, S. D. M. 1997, *ApJ*, **490**, 493
- Oñorbe, J., Boylan-Kolchin, M., Bullock, J. S., et al. 2015, *MNRAS*, **454**, 2092
- Orkney, M. D. A., Read, J. I., Rey, M. P., et al. 2021, *MNRAS*, **504**, 3509
- Orkney, M. D. A., Taylor, E., Read, J. I., et al. 2023, arXiv:2302.12818.
- Peebles, P. J. E. 2021, arXiv:2106.02672.
- Peñarrubia, J., Pontzen, A., Walker, M. G., & Koposov, S. E. 2012, *ApJL*, **759**, L42
- Plastino, A. R., & Plastino, A. 1993, *PhLA*, **174**, 384
- Putko, J., Sánchez Almeida, J., Muñoz-Tuñón, C., et al. 2019, *ApJ*, **883**, 10
- Read, J. I., Agertz, O., & Collins, M. L. M. 2016, *MNRAS*, **459**, 2573
- Read, J. I., Walker, M. G., & Steger, P. 2019, *MNRAS*, **484**, 1401
- Roychowdhury, S., Chengalur, J. N., Karachentsev, I. D., & Kaisina, E. I. 2013, *MNRAS: Lett.*, **436**, L104
- Sánchez Almeida, J. 2022, *Univ*, **8**, 214
- Sánchez Almeida, J., Elmegreen, B. G., Muñoz-Tuñón, C., & Elmegreen, D. M. 2014, *A&ARv*, **22**, 71
- Sánchez Almeida, J., Filho, M. E., Dalla Vecchia, C., & Skillman, E. D. 2017, *ApJ*, **835**, 159
- Sánchez Almeida, J., & Trujillo, I. 2021, *MNRAS*, **504**, 2832
- Sánchez Almeida, J., Trujillo, I., & Plastino, A. R. 2020, *A&A*, **642**, L14
- Sánchez Almeida, J., Trujillo, I., & Plastino, A. R. 2021, *ApJ*, **921**, 125
- Sánchez-Janssen, R., Ferrarese, L., MacArthur, L. A., et al. 2016, *ApJ*, **820**, 69
- Smoot, G. F., Bennett, C. L., Kogut, A., et al. 1992, *ApJL*, **396**, L1
- Spergel, D. N., & Steinhardt, P. J. 2000, *PhRvL*, **84**, 3760
- Strigari, L. E., Frenk, C. S., & White, S. D. M. 2017, *ApJ*, **838**, 123
- Trujillo, I., D'Onofrio, M., Zaritsky, D., et al. 2021, *A&A*, **654**, A40
- Virtanen, P., Gommers, R., Oliphant, T. E., et al. 2020, *NatMe*, **17**, 261
- Weinberg, D. H., Bullock, J. S., Governato, F., Kuzio de Naray, R., & Peter, A. H. G. 2015, *PNAS*, **112**, 12249
- White, S. D. M., & Rees, M. J. 1978, *MNRAS*, **183**, 341